REVIEW SUMMARY

NANOPHOTONICS

Miniaturization of optical spectrometers

Zongyin Yang*, Tom Albrow-Owen*, Weiwei Cai†, Tawfique Hasan†

BACKGROUND: Optical spectrometry is one of the most powerful and widely used characterization tools in scientific and industrial research. Benchtop laboratory spectrometer systems—characterized by bulky optical components, moving parts, and long path lengths—can deliver unparalleled, ultrafine resolution and wide spectral ranges. However, a rapidly growing application space exists for spectral analysis where the need for reduced physical dimensions, cost, or power consumption takes precedence over the need for high performance. The demand for portable or handheld spectral analysis devices requires shrinking of these systems down to centimeter-scale footprints. More extreme miniaturization to submillimeter length scales would open a range of opportunities for in situ analysis, with potential for integration into lab-on-a-chip systems, smartphones, or even spectrometer-per-pixel snapshot hyperspectral imaging devices. Toward this aim, an approach that involves simply scaling down benchtop systems (with miniaturized gratings and reflective optics) becomes constrained as a result of the complex fabrication involved and the inherent proportionality of resolution to path length in dispersion-based systems.

ADVANCES: A wide variety of miniaturized spectrometer systems have emerged since the early 1990s. These can be grouped into four broad categories according to the underlying strategies they use for spectral characterization: (i) those that have tried to push the boundaries of miniaturization using a conventional benchtop strategy, where light interacts with miniaturized dispersive optics such that different spectral components are spatially separated when arriving at a detector array; (ii) narrowband filters, which can be used to selectively transmit light with specific wavelengths, such that analysis of complete spectra can be achieved either with a single filter (the transmissive properties of which can be varied over time) or by passing light through an array of multiple unique narrowband filters, each mounted onto its own detector; (iii) Fourier transform systems, where integrated interferometers [such as those based on microelectromechanical systems (MEMS) components] can be used to produce temporal or spatial interferograms, which are then computationally converted to a readable spectrum; and (iv) a newly emerging paradigm of microspectrometers, in which computational techniques are used to approximate or reconstruct an incident light spectrum from precalibrated spectral response information encoded within a set of broadband detectors or filters.

OUTLOOK: We now stand at a watershed where this field is yielding ultracompact microspectrometer systems with performance and footprint near those viable for integrated applications such as lab-on-a-chip systems, smartphones, and spectral imagers. Until recently, advancement has been inspired by and has benefited from wider technological trends in the production of hardware. For instance, earlier dispersion-based strategies have been improved through optimization of high-precision microfabrication, lithographic, and etching techniques to produce ever more scaled-down gratings and optics. In parallel, the development of MEMS components has enabled ultracompact, electronically driven moving parts for miniaturized Fourier transform interferometer–based devices. However, as the physical size and cost of processing power have fallen sharply over the past 15 years, the emergence of reconstructive microspectrometers has heralded a fundamental shift in the field, where developments in the software will shoulder much of the burden for enhancing device performance while footprints continue to shrink. Maturation of the algorithmic strategies behind these devices will likely see the incorporation of machine learning–based techniques, which increasingly will be able to compensate for the compromises in detector performance necessitated by further miniaturization. This represents a promising route toward ultracompact high-performance systems and the emergence of spectral analysis in a host of previously inaccessible platforms in scientific research, industry, and consumer electronics. ■

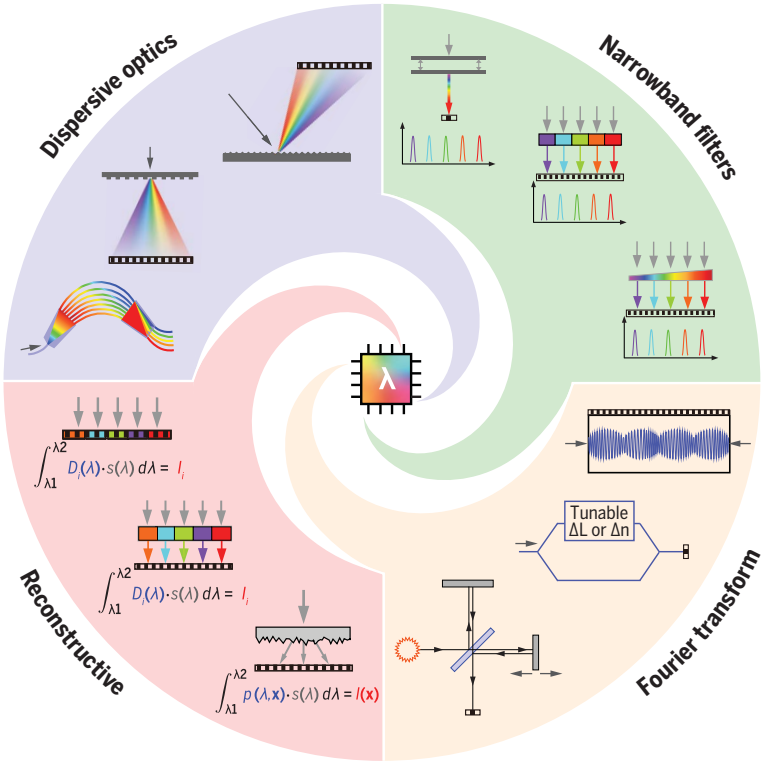

Strategies toward ultracompact microspectrometers. Schemes for miniaturized spectral sensing systems based on dispersive optics, narrowband filters, Fourier transform interferometers, and computational spectral reconstruction schemes have all emerged over the past three decades.

The list of author affiliations is available in the full article online.
*These authors contributed equally to this work.
†Corresponding author. Email: cweiwei@sjtu.edu.cn (W.C.); th270@cam.ac.uk (T.H.)
Cite this article as Z. Yang *et al.*, *Science* **371**, eabe0722 (2021). DOI: 10.1126/science.abe0722

REVIEW

NANOPHOTONICS

Miniaturization of optical spectrometers

Zongyin Yang[1,2]*, Tom Albrow-Owen[1]*, Weiwei Cai[3]†, Tawfique Hasan[1,4]†

Spectroscopic analysis is one of the most widely used analytical tools in scientific research and industry. Although laboratory benchtop spectrometer systems offer superlative resolution and spectral range, their miniaturization is crucial for applications where portability is paramount or where in situ measurements must be made. Advancement in this field over the past three decades is now yielding microspectrometers with performance and footprint near those viable for lab-on-a-chip systems, smartphones, and other consumer technologies. We summarize the technologies that have emerged toward achieving these aims—including miniaturized dispersive optics, narrowband filter systems, Fourier transform interferometers, and reconstructive microspectrometers—and discuss the challenges associated with improving spectral resolution while device dimensions shrink ever further.

Optical spectrometers have served as one of the most important instruments to date for materials characterization and chemical analysis (*1*). Conventional benchtop spectrometers typically rely on a combination of bulky dispersive optics, long optical path lengths, detector arrays, and movable parts. These requirements impede their miniaturization for applications where it is critical to minimize size, cost, and power consumption. Recent years have seen the development of scaled-down spectrometer systems for a wide range of handheld, portable, and integrated applications, including soil and crop analysis, monitoring of food industry production lines, and marine/underwater scientific research (*2*–*6*). It is clear that in these uses, it is often far preferable to attain indicative, instantaneous, on-the-spot results, rather than transporting samples to a laboratory for ultrahigh-resolution analysis (*5*, *7*). Further miniaturization, down to the submillimeter scale, could provide opportunities in a wide range of applications, including lab-on-a-chip spectroscopy and other in situ or even in vitro characterization systems. Various possibilities can be envisaged for consumer technologies, such as in smartphone-based devices (*8*, *9*), for applications including the detection of counterfeit pharmaceuticals and banknotes, monitoring of skin health, or even determining the sugar and fat content in food products. On the other hand, in industry, devices suitable for drone-based spectral imaging—that is, where spectral information is correlated with spatial data—could revolutionize large-scale crop monitoring.

In general, reducing the size of a spectrometer necessitates a compromise with respect to degradation of its resolution, dynamic range, or signal-to-noise ratio. However, microspectrometers can be engineered to meet "acceptable" levels of performance for specific applications (*7*, *10*). In many cases, where the goal is identification of signature spectral peaks rather than relative metrology, a "satisfactory" resolution in the visible range may, for instance, be on the order of 10 nm, or even larger (*5*). Moreover, by enhancing a particular aspect of performance, microspectrometers can be specialized for extreme measurements that are challenging to implement using a conventional system. For example, the relative strengths of on-chip single-photon spectrometers (*11*, *12*) and single-nanowire spectrometers (*13*) lie in their ultrahigh-sensitivity detection and ultracompact footprint, respectively.

Since the early 1990s, miniaturized optical spectrometers based on a wide variety of designs and working principles have been demonstrated, with a range of operational spectral bands and resolutions. Below, we summarize the most explored technological platforms, presenting their relative merits and drawbacks. We have broadly organized the field into four main categories, representing the most prominent strategies for identifying different spectral components. The first three categories are (i) those that feature dispersive optics to split light toward spatially separated detectors (Fig. 1A), (ii) those that use narrowband filters to preferentially transmit particular spectral components to different detectors (Fig. 1B), and (iii) Fourier transform microspectrometers based around temporal or spatial interferometers (Fig. 1C). Early miniaturized spectrometers fell within these first three classifications and featured designs that largely resembled scaled-down benchtop spectrometers, with out-of-plane diffractive optics or microelectromechanical systems (MEMS)–based interferometers. Further development saw such designs largely give way to planar systems based on waveguides and integrated optics (*14*–*19*).

However, in the past decade, a fourth category has emerged as a new paradigm of microspectrometer devices. "Reconstructive" or "computational" spectrometer systems (Fig. 1D) take advantage of more readily available computer processing power and reductions in microprocessor size and cost. They typically feature a set of detectors encoded with distinctive spectral response characteristics, which, when measured in parallel, can be combined using complex algorithms to approximate or "reconstruct" an incident light spectrum. Such systems can harness not only technological advances in hardware, but also the development of new computational approaches—in particular, those based on compressive sensing and machine learning.

Miniaturized dispersive optics

Conventional spectrometers typically consist of one or several diffraction gratings, an optical path, and a detector array. Light passes through an input slit and is collimated onto a diffraction grating that disperses spectral components in different directions. A concave mirror focuses this dispersed light toward the detector array. Advancements in micro- and nanofabrication techniques have provided an opportunity to develop microspectrometers by scaling down the components of these systems. A wide range of increasingly miniaturized, spatially dispersive spectrometers with centimeter-scale footprints have been demonstrated since the 1990s (*20*, *21*). These dispersive microspectrometers have typically been fabricated via wafer bonding, with optical paths fashioned through electrochemically controlled etching (Fig. 2A).

As the system footprint and thus the component size decreases, a number of factors must be considered. Separation of spectral components at the detector plane depends on the distance light is allowed to travel after meeting the dispersive element. As such, for a given grating and detector array, the resolution $\Delta\lambda$ [the full width at half maximum (FWHM) of the narrowest distinguishable spectral component, in nanometers] is proportional to the optical path length of the system. When the device is made more compact, the path length also necessarily decreases, thus lowering the spectral resolution. This can be compensated to an extent by increasing the detector's pixel density within a given width.

[1]Department of Engineering, University of Cambridge, Cambridge CB3 0FA, UK. [2]College of Information Science and Electronic Engineering, State Key Laboratory of Modern Optical Instrumentation, Zhejiang University, Hangzhou 310027, China. [3]Key Laboratory of Education Ministry for Power Machinery and Engineering, School of Mechanical Engineering, Shanghai Jiao Tong University, Shanghai 200240, China. [4]Cambridge Graphene Centre, University of Cambridge, Cambridge CB3 0FA, UK.
*These authors contributed equally to this work.
†Corresponding author. Email: cweiwei@sjtu.edu.cn (W.C.); th270@cam.ac.uk (T.H.)

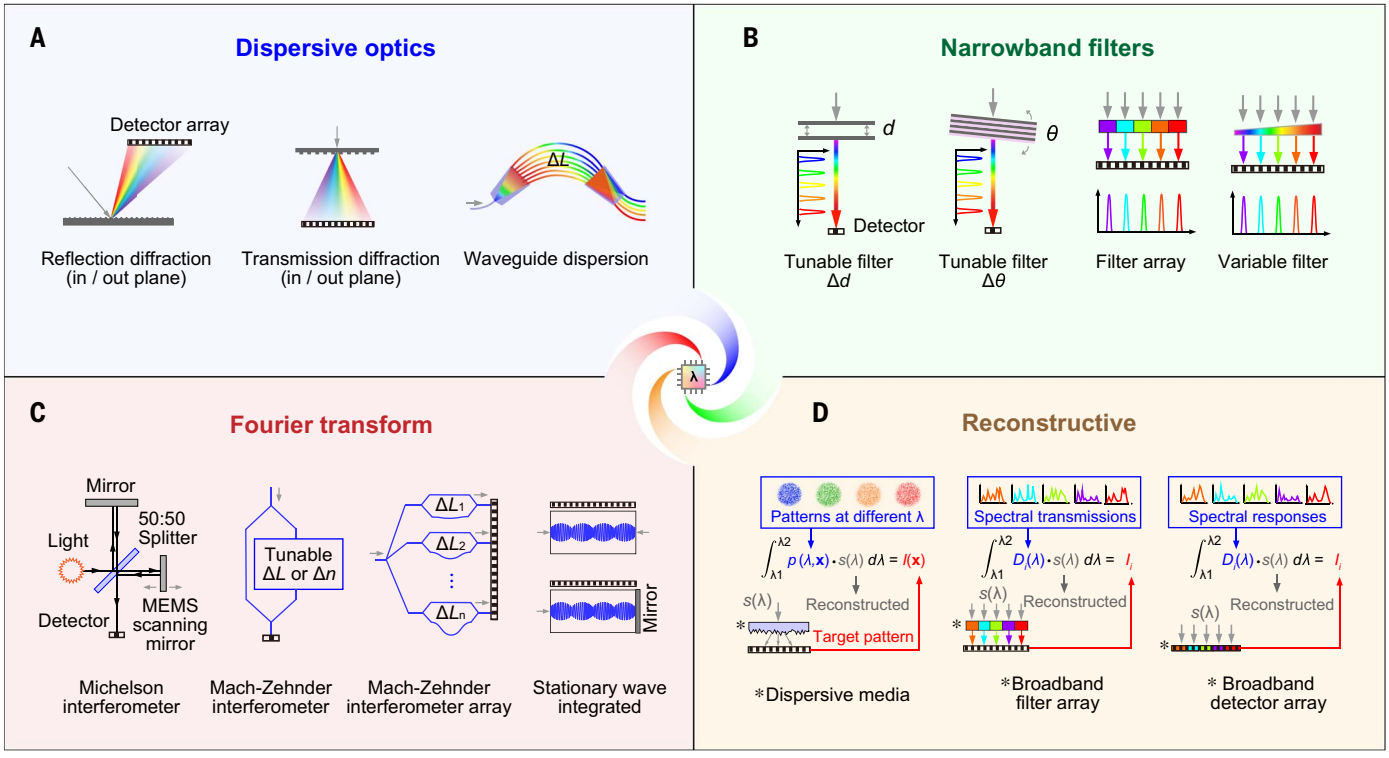

Fig. 1. Different underlying strategies for miniaturized spectrometer systems that have emerged over the past 30 years. (**A**) Miniaturized dispersive optics. (**B**) Tunable or arrayed narrowband filters. (**C**) Fourier transform–based systems. (**D**) Computational spectral reconstruction–based systems.

However, the quality of optical components and the system alignment present conflicting problems in fabrication; for instance, etching-induced surface roughness will cause more light to be scattered before arriving at the detector array (*21*).

Furthermore, the resolution will be affected if there are no collimation components to image the input slit onto the detector. A feasible approach is to use a concave grating (*6*, *22*, *23*); light is then dispersed and focused from different angles to different positions on the detector array without the need for complex collimation optics and multiple reflective components (Fig. 2B) (*23*). Commercial, manufacturable, visible-range microspectrometers based on this design have achieved a resolution of ~10 nm with a footprint of 1 to 2 cm (*23*). In addition to these concave gratings, meta-lenses (*24*) and grating-Fresnel lenses (*25*) have been demonstrated as diffractive optical elements. The grating-Fresnel lens—an integrated combination of a diffraction grating and Fresnel lens—has also been developed within a smartphone-attached spectrometer system (Fig. 2C) (*9*).

Waveguides have been proposed as an alternative to free-space optics, allowing more compact light confinement, to further reduce footprint without considerable compromise on performance (*14*). For this approach, input and output gratings are etched on the two sides of the substrate, followed by deposition of a waveguide layer on top. As illustrated in Fig. 2D, in these systems, light is coupled into the waveguide via an input grating. When propagating through the waveguide, light interacts with analytes on the waveguide surface. A photodetector array then detects the light upon its exit from an output grating. As such, the system can be used to measure incident light spectra or the absorption spectra of the analytes on top of the waveguide through evanescent coupling.

These waveguide-based spectrometers have used various dispersion schemes (Fig. 2, E to I) such as planar photonic crystals (*18*, *26*), holographic elements (*19*, *27*), planar echelle gratings (*12*, *28*), transmission gratings (*29*), self-focusing transmission gratings (*16*), chirped gratings (*30*), and arrayed waveguide gratings (AWGs) (*17*), as well as metasurfaces (*31*). As with the out-of-plane devices, the resolution of waveguide-based spectrometers is inherently tied to the optical path length afforded by the system's footprint, and as such, miniaturization necessitates a reduction in performance. Furthermore, with respect to manufacturability, fabrication tolerances (for example, in relation to sidewall roughness–induced losses) and waveguide mode coupling at low channel spacings present a challenge for extreme miniaturization below the millimeter scale (*32*, *33*). However, aside from greater light confinement, advantages present themselves in their straightforward integration into monolithic, waveguide-based optical analysis systems.

In addition to innovations with respect to configuration and dispersive elements, simultaneously decreasing the size and increasing the sensitivity of the photodetector arrays provides another route toward smaller, higher-performance microspectrometers. For example, superconducting nanowires have recently emerged as one of the most promising alternatives to semiconductor photodetectors for spectrometer applications, as they show ultrahigh sensitivities (single-photon detectability) with low jitter and dark counts (*11*, *12*). Indeed, recent single-photon microspectrometer demonstrations using superconducting nanowires are capable of carrying out spectral analysis of ultrafaint light, which marks a step toward their use in astronomical spectroscopy and quantum computing (*11*, *12*).

Narrowband filters

Narrowband filters selectively transmit light with specific wavelengths, allowing for their use in spectrally selective detection. In these systems, light dispersion can be achieved either with a single filter, the transmissive properties of which can be varied over time, or by passing light through an array of multiple unique narrowband filters each mounted onto their

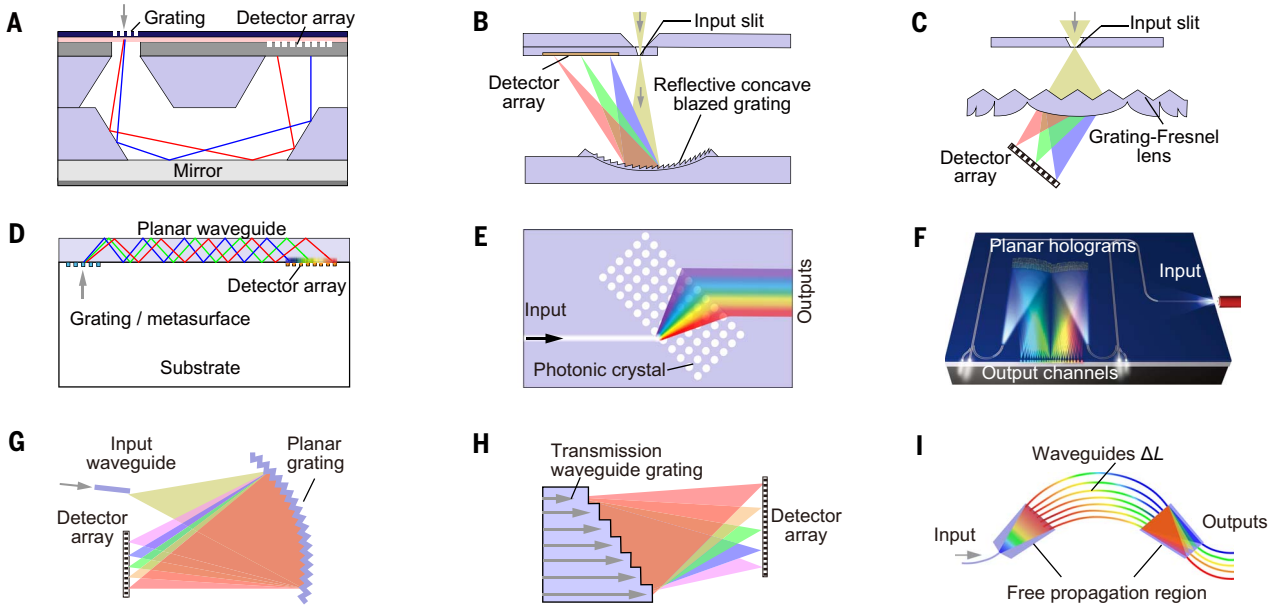

Fig. 2. Spatially dispersive microspectrometers. (**A** and **B**) Miniaturized spectrometer systems based on out-of-plane spatial dispersion using planar (*21*) and concave (*23*) gratings, respectively. (**C**) Schematic of a grating-Fresnel spectrometer (*9*). (**D** to **I**) Waveguide-based spectrometers based around different dispersion elements: (D) a buried grating on a waveguide sensor (*14*), (E) a photonic crystal–based grating (*18*), (F) a holographic element (*19*), (G) a planar echelle grating (*28*), (H) a transmission waveguide grating (*16*), and (I) an arrayed waveguide grating (*17*). [(F) adapted with permission from (*19*).]

own detector. Although they are still limited by the detector and filter size, narrowband filter-based spectrometers offer a key advantage with respect to miniaturization over those based on dispersive systems. Aside from the benefit of their planarity, no separation (that is, path length) is required between the spectral filtering element(s) and the detector(s), circumventing one of the fundamental limitations of dispersive devices and affording the possibility of far more compact systems.

Tunable filter–based microspectrometers

A range of tunable narrowband filters, such as acousto-optic tunable (AOTF) (*34*), liquid-crystal tunable (LCTF) (*35*), and Fabry-Pérot (*36*–*38*) filters, as well as microring resonators (*39*) have all been demonstrated in spectrometers. Their spectral transmission can be rapidly and dynamically controlled through the application of a voltage or acoustic signal that temporally separates spectral components. AOTFs use an acoustic field to generate a periodically fluctuating refractive index in solid-state birefringent crystals, analogous to a tunable diffraction grating. However, to date, size constraints on the birefringent crystals have presented a major obstacle to AOTF spectrometer miniaturization. LCTFs suffer from a similar constraint, containing a stack of polarizers and liquid crystal cells that are challenging to miniaturize. On the other hand, tunable Fabry-Pérot filters can be fabricated by well-established MEMS-compatible processes (*40*), which make them highly suitable for microspectrometer mass production (*4*, *37*).

A typical structure for a tunable Fabry-Pérot filter–based microspectrometer (Fig. 3A) features a resonant optical cavity consisting of two parallel mirrors separated by a variable distance d. The transmission function T of the Fabry-Pérot filter is given by the Airy function (*41*):

$$T = \frac{\left(1-\frac{A}{1-r}\right)^2}{1+\frac{4r}{(1-r)^2}\sin^2\left[\frac{2\pi}{\lambda}(nd\cos\theta)-\varphi\right]} \quad (1)$$

where A is the absorbance of mirrors and cavity, r is the reflectance of the mirrors, n is the refractive index of the cavity medium, θ is the incidence angle, and φ is the phase shift at the reflectors, which normally is neglected. Light can be resonated and enhanced in the cavity when the optical distance between the two mirrors ($nd\cos\theta$) is an integral multiple of its half wavelength $\lambda/2$, which results in maximum ideal transmission through the cavity (and reflector) to the detector ($T = 1$). Figure 3A shows T as a function of light wavelength. Assuming that the absorbance and reflectance are fixed for a given device, transmission spectra can be tuned during operation by varying the optical path length, which can be achieved by changing n, d, or θ. Tuning the separation of the mirrors (Δd) is the most common strategy and is achieved through the use of an electrostatic or piezoelectric actuator (Fig. 3, B and C), where current MEMS technology straightforwardly affords a wide tunable range (*36*, *37*, *41*, *42*). Tunability of the refractive index Δn can be realized by choosing electro-optically tunable $LiNbO_3$ (*43*, *44*) or liquid crystals (*45*) as the cavity medium; the angle of incidence $\Delta\theta$ has been varied via rotating the filter (*46*).

There are certain key factors to consider in engineering these Fabry-Pérot spectrometers for high performance. The FWHM of transmission peaks determines the spectral resolution of the filter-based spectrometers, which in turn is equal to the intrinsic finesse of the cavity $F_{int} = \pi\sqrt{r}/(1-r)$ (*20*). Thus, high resolution requires high reflectance, but for a metallic mirror cavity, this results in lower transmission and therefore a weaker signal-to-noise ratio (*37*). A partial solution here is to use distributed Bragg reflectors as mirrors (*47*), which consist of alternating high– and low–refractive index dielectric quarter-wave layers with high reflectance and low absorption at a specific spectral range. However, they are costly and much more complex to manufacture. Note that defects in the cavity system, including nonparallelism or mirror imperfections, also reduce the effective finesse (and thus resolution):

$$\frac{1}{F_{eff}^2} = \frac{1}{F_{int}^2} + \frac{1}{F_D^2} \quad (2)$$

where F_D represents the defect finesse (*20*).

Filter arrays and linear variable filters

For the tunable narrowband filter spectrometers discussed above, the spectra are analyzed in a time sequence, sacrificing time response. This also presents an obstacle for high-speed

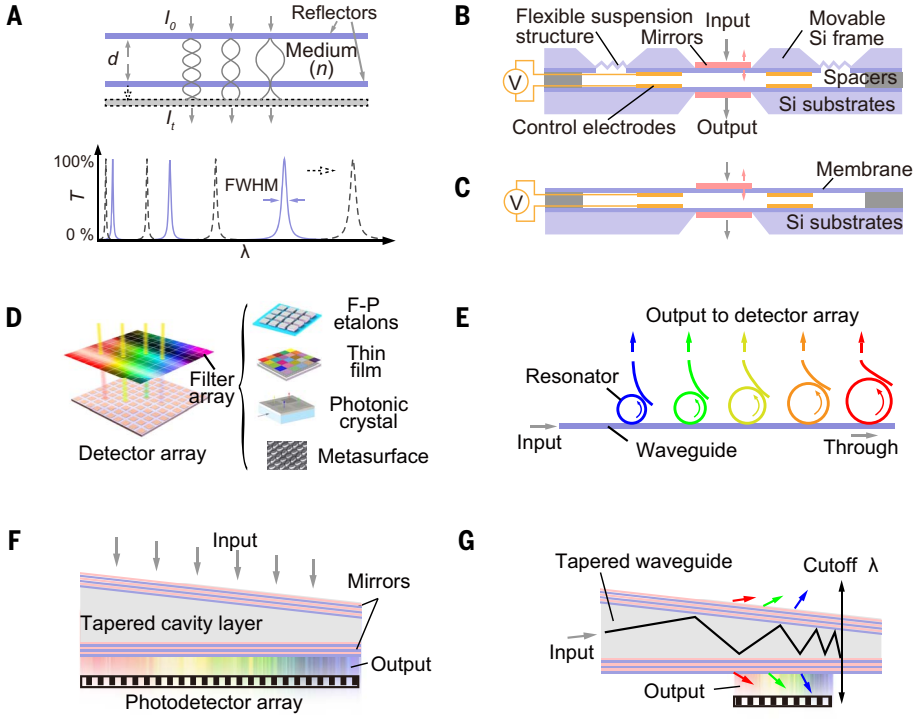

Fig. 3. Narrowband filter spectrometers. (**A**) Schematic configuration (top) and the corresponding transmittance function (bottom) of a typical Fabry-Pérot filter. (**B** and **C**) Typical configurations of tunable Fabry-Pérot filter–based microspectrometers showing a bulk wafer bonding structure (*42*) and a membrane-on-wafer structure (*4*), respectively. (**D**) Schematic of a filter array microspectrometer scheme based around Fabry-Pérot etalons (*49*), etched thin films (*51*), photonic crystals (*52*), and metasurface (*54*). (**E**) A waveguide ring resonator–based filter strategy. (**F** and **G**) Schematic of linear variable filter–based spectrometer designs and their implementation, for transverse incidence (*60*) and waveguided operation (*61*), respectively. [Metasurface image at lower right of (D) adapted with permission from (*54*).]

spectroscopy applications. Narrowband filter arrays and linear variable filters offer an advantage in allowing simultaneous measurement of multiple spectral components in parallel (although this in turn necessitates multiple detectors).

Fixed filter arrays have been exploited in many microspectrometers, where each filter is responsible for transmitting a specific wavelength onto the photodetector underneath. Various filter schemes exist, differentiated by their working principles, configurations, and materials (*48*). Filter arrays based on Fabry-Pérot etalons (*49*, *50*), thin films (*51*), planar photonic crystals (*52*), photonic bandgap fibers (*53*), metasurfaces (*54*), and waveguide ring resonators (*39*) have been demonstrated for the development of microspectrometers (Fig. 3, D and E). Clearly, the number of channels directly constrains the spectral resolution [in the case of the 16 filters in (*49*), for example, to ~25 nm], so processes that necessitate the individual placement or deposition of each filter are ill-suited. To address this, a combinatorial deposition technique can be used to fabricate a large number of filters in fewer steps; for example, an 8 × 16 array (128 channels) can be fabricated in only nine deposition processes (*51*).

Another strategy to increase the ease of fabricating a wide range of transmission wavelengths is to use a linear variable filter, which is typically either a wedged (*55*, *56*) or composition-graded filter (*57*), where the transmission or reflection spectrum varies continuously along one axis of the filter. One approach here is to simply scan a spectrum by sliding the filter over a single detector (*58*). However, this is relatively slow and necessitates extra moving parts. Combining a linear variable filter with a detector array for parallel measurement offers an ideal solution (*59*). Microspectrometers based on this configuration have already been demonstrated (Fig. 3F) (*60*). Tapered Bragg waveguides exhibit similar linear variable filtering capability due to the variable cutoff propagation wavelength (Fig. 3G) (*61*). Both linear variable configurations show high spectral resolution (~1 nm).

Fourier transform microspectrometers

Typically used for absorption or emission spectroscopy in the infrared range, Fourier transform (FT) spectrometers center around the use of an interferometer to modulate the light incident on a single detector over time. The "interferograms" collected at the detector (functions of received signal intensity over time, or a time-variant property of the system such as optical path length) are then converted to a wavelength-dependent spectrum via FT. FT systems have two main inherent benefits over those based on diffractive optics. First, collecting spectral information at one detector simultaneously results in the multiplex (or Fellgett's) advantage. Second, avoiding spatial dispersion results in a higher optical throughput, or étendue, known as Jacquinot's advantage. Both of these factors tend toward affording a higher signal-to-noise ratio. Moreover, using one detector offers a smaller and more cost-effective alternative to array-based detectors.

Miniaturized FT spectrometers can be categorized through the mechanism by which the optical path lengths within the interferometer are changed over time; the broadest differentiation is between those with and without moving parts. Belonging to the former group, the earliest chip-based FT spectrometers, appearing first in the late 1990s, were based around Michelson interferometers, with MEMS used to manipulate mirrors with either electrostatic (*62*–*64*), electromagnetic (*65*), or electrothermal (*66*) (often comb-drive) actuators (Fig. 4A). Aside from difficulties in integration with planar light sources, a drawback of these devices is that the spectral resolution is limited by the maximum optical path length difference (OPD) allowed by the actuator travel range (*67*), which in turn is constrained by, for instance, the pull-in effect (whereby, below a threshold separation, the mirrors will uncontrollably and rapidly attract each other) (*2*, *6*). Very recently, it has been demonstrated that the evaporation of a droplet atop the end of an optical fiber can also function as a system analogous to a scanning FT spectrometer, to obtain the absorption spectra of liquid analytes (*68*).

As of the late 2000s, planar on-chip FT spectrometers—based on integrated waveguides and without movable mirrors—have emerged. Instead of Michelson architectures, these systems are based around Mach-Zehnder interferometers (MZIs), whereby light is split into at least two unidirectional pathways toward a single detector where they are recombined. Here, the OPD induces a phase difference between light in different channels. Some of these systems are based around arrays of multiple MZIs, forming spatial heterodyne spectrometers (*69*–*71*). For instance, an array of spirally coiled waveguides was fabricated (Fig. 4B), with the length of the waveguides varying linearly by ΔL, inducing a delay between the paths (*70*). However, such a system is limited by the maximum OPD as well as the number of MZIs, both of which constrain

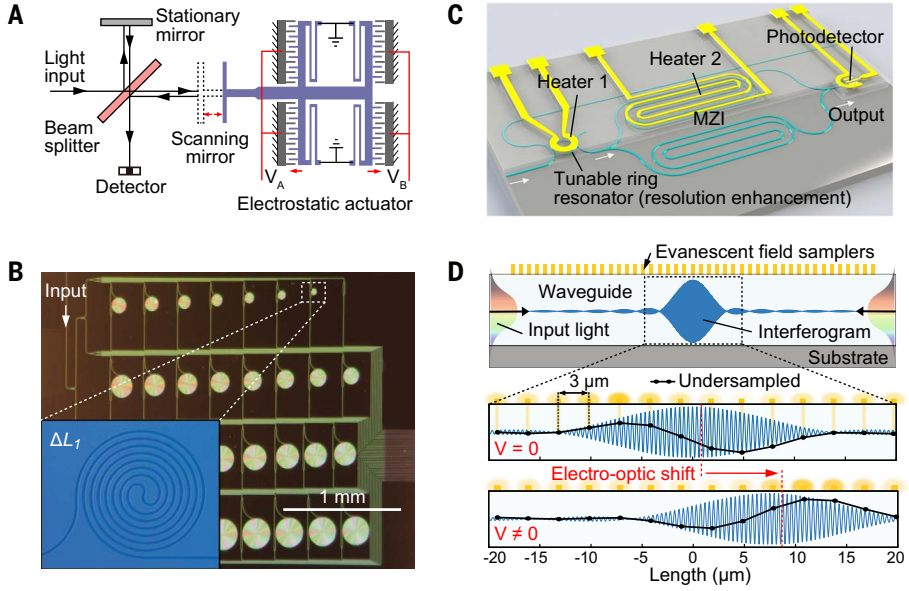

Fig. 4. Fourier transform microspectrometer platforms. (**A**) Schematic of a miniaturized MEMS Fourier transform spectrometer based on a Michelson interferometer. The path lengths of the interferometer are varied over time by the electrostatic actuator to collect an interferogram, which is subsequently converted to spectral data by Fourier transform (*62*). (**B** and **C**) MZI-based, on-chip Fourier transform spectrometers. (B) Optical image of a spatial heterodyne spectrometer device based on an array of multiple MZIs with different OPDs, each varying by ΔL_i. (C) Schematic of a microspectrometer based on a single MZI, using a microring resonator for resolution enhancement and a heater to facilitate path length modulation by thermo-optical effect. [(B) and (C) adapted with permission from (*70*, *74*), respectively.] (**D**) Schematic (top) of a standing-wave integrated Fourier transform spectrometer system in an electro-optically tunable medium; diagrams (below) illustrate the use of the electro-optic effect in $LiNbO_3$ to shift the interferogram along the waveguide over time through application of a bias voltage *V*. [Adapted with permission from (*79*).]

the extent to which the spectrometer footprint can be reduced while maintaining satisfactory performance.

Building on this, alternative designs use mechanisms that can continuously tune the characteristics of a single MZI (and thus require only a single photodetector) rather than relying on multiple MZIs with fixed lengths. This has been achieved through electro-optical modulation in, for example, $LiNbO_3$ waveguides (*67*, *72*) as well as through exploiting thermo-optical effects, where microheaters are embedded adjacent to integrated optical pathways (*73*, *74*) (Fig. 4C). An alternative approach is a digital FT spectrometer, where a photonic circuit is used, featuring a number of optical switches that divert the signal along paths of different lengths (*75*). Here, the resolution depends on the number of paths, or spectral channel count, which scales exponentially with the number of optical switches. In many of these methods, recent advances have allowed computational techniques such as compressive sensing (*71*), machine learning (*76*), and forward-backward linear prediction (*67*) to enhance the spectral resolution of these devices and correct for temperature change– or fabrication-based errors.

A related variant of these miniaturized interferometer–based FT systems is stationary wave integrated Fourier transform spectrometry (SWIFTS). In recent works on SWIFTS-based microspectrometers, a standing wave is set up within a single-mode, closed-loop waveguide through the interference of two counterpropagating signals (alternatively, in a Lippmann configuration, a mirror can be placed at the end of a waveguide to set up a standing wave by reflecting the signal back upon itself) (*77*, *78*). Whereas temporal interferograms are produced and collected at a single detector in the previously mentioned FT spectrometers, here a spatial interferogram is produced. Metallic nanoribbons are deposited with a regular spacing on top of the waveguide to sample the evanescent field and map the relative intensity of the standing wave along the loop (Fig. 4D). A proof-of-concept demonstration for this design acknowledged that the spectral range in such a system is constrained (in this case, to 96 nm centered at 1500 nm), as the samplers cannot be fabricated at a pitch to avoid undersampling of the interferogram (*77*).

However, more recently, a SWIFTS system has been developed that circumvents this issue using a dual spatial and temporal sampling scheme. Use of the electro-optic effect in a hybrid $LiNbO_3$-SiN waveguide platform allows the spatial interferogram to be shifted along the waveguide by applying a voltage (Fig. 4D) such that, even with a fixed array of nanosamplers, the whole interferogram can be sampled, in this case achieving a spectral range of 500 nm (*79*). The resolving power, $R = \lambda/\Delta\lambda$, in these devices is given by $2nL/\lambda$, where n is the refractive index of the waveguide, L is the length of waveguide being probed, and λ is the wavelength. As such, extremely high resolutions (tens of picometers) are possible over only centimeter length scales, although, conversely, such devices may not be suitable for extreme miniaturization. These systems also currently rely on an external camera to image the interferogram scattering from the samplers; the development of specialized nanoscale photodetectors, to be placed on top of the waveguide, would allow for direct measurement and a simplified system.

Reconstructive spectrometers

Over the past decade, a new spectrometer paradigm has emerged, which, as indicated by the name, relies on computational techniques to approximate or "reconstruct" an incident light spectra from precalibrated information encoded within a set of detectors. More specifically, the "reconstruction" here refers to the solution of a linear equation system. Thus far, two strategies have generally been seen for encoding spectral information within a set of detectors: complex spectral-to-spatial mapping and spectral response engineering.

Complex spectral-to-spatial mapping

In a conventional grating-based spectrometer, a point (i.e., a wavelength) in the spectral domain is mapped to a point (i.e., a detector) in the spatial domain (*80*). The readout of the detectors directly constitutes the spectrum. However, as mentioned previously, the spectral resolution scales with the distance from the grating to the detectors (i.e., the path length); one-to-one spectral-to-spatial mapping is thus highly limited when looking to increase spectral resolution with a decreasing footprint (*81*). Complex spectral-to-spatial mapping is an alternative approach that distinguishes the wavelengths by creating a signature pattern (either one- or two-dimensional) in the spatial domain for each of the wavelengths (Fig. 5A). For example, when monochromatic light passes through a dispersive element such as a long multimode fiber (MMF), it will create a wavelength-dependent signature pattern at the output of the fiber due to the interference between the guided modes in the fiber (*80*). Thus, when passing an arbitrary polychromatic light through the MMF, the output will be the overlay of scaled signature patterns created by each of the individual wavelengths. The target spectrum to be reconstructed is essentially the assembly of scaling weights corresponding to these patterns (*81*). The signature patterns can also be generated by feeding the light into a

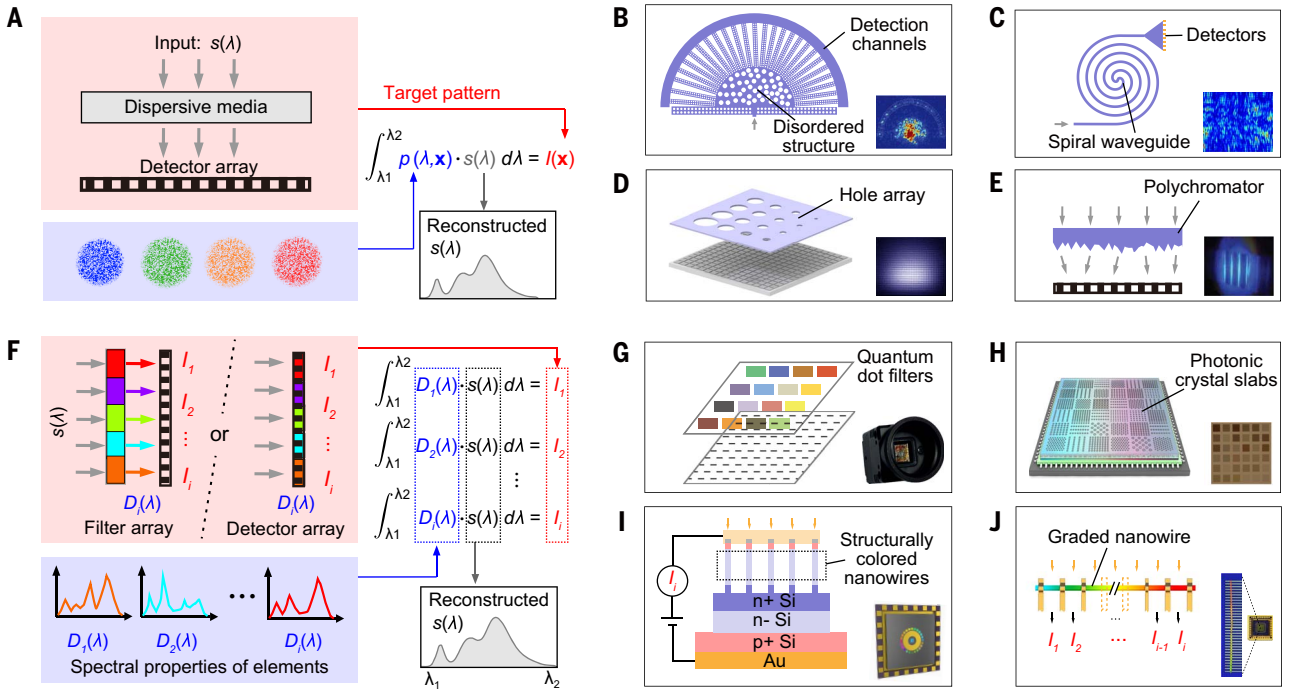

Fig. 5. Computational microspectrometers. (**A**) Operational principles behind spectrometers based on spectral-to-spatial mapping. (**B** to **E**) Examples of optical systems that had been adopted for complex spectral-to-spatial mapping: (B) a disordered photonic chip, (C) a spiral waveguide, (D) a dispersive hole array, or (E) a polychromator. [(B) to (E) adapted with permission from (*81*, *83*–*85*), respectively.] (**F**) Principles behind reconstructive spectrometers based on engineered spectral response filtering or detection. (**G** to **J**) Examples of different reconstructive systems using spectrally engineered filtering, with arrays based on colloidal quantum dot mixtures (G) and photonic crystal slabs (H), and spectrally engineered detection, based on arrays of structurally colored nanowires (I) and a single compositionally engineered nanowire (J). [(G) to (J) adapted with permission from (*86*), (*88*), (*95*), and (*13*), respectively.]

miniaturized optical element such as a disordered photonic chip (*81*, *82*), a spiral waveguide (*83*), a dispersive hole array (*84*), or a polychromator (*85*) (Fig. 5, B to E). For a sought spectrum $s(\lambda)$ with normalized signature patterns $p(\lambda, \mathbf{x})$ and signals measured at the detector array $I(\mathbf{x})$, the mapping process can be mathematically described as

$$I(\mathbf{x}) = \int_{\lambda_1}^{\lambda_2} p(\lambda, \mathbf{x}) \cdot s(\lambda) d\lambda \qquad (3)$$

where $\mathbf{x}$ is a vector denoting a position on the detector array. Equation 3 can be discretized as

$$\mathbf{I} = \mathbf{P} \cdot \mathbf{S} \qquad (4)$$

where $\mathbf{I}$, $\mathbf{S}$, and $\mathbf{P}$ are the measured intensity, spectrum, and mapping matrices, respectively.

If the signature patterns of two distinct wavelengths are identical, it is impossible to tell which wavelength leads to the measured pattern. In this way, the dissimilarity between the signature patterns determines the resolving power of the reconstructive spectrometers. Mathematically, the signature patterns are the columns of the matrix $\mathbf{P}$; the higher the similarity between the signature patterns, the larger the condition number of $\mathbf{P}$, leading to a poorer numerical solution of Eq. 4. As a result, the signature patterns should be as diverse as possible. It has been recognized that the diversity is proportional to the spread of the optical path length (i.e., the difference between the shortest and longest optical paths of the propagation modes within the chosen optical elements) (*81*). A resolution of 0.01 nm has been demonstrated with a multimode spiral waveguide that uses evanescent coupling to considerably enhance the optical path length spread (*83*). Such a high resolution can greatly broaden the applications of miniaturized spectrometers. In addition, these systems are robust with respect to fabrication imperfections, which can be compensated for through calibration (*83*). However, they suffer from temperature variations, which can change the signature pattern for a specific wavelength. The higher the spectral resolution, the more the spectrometer suffers from thermal instability. Thus, additional measures such as adding a temperature controller or temperature-dependent calibration should be adopted (*83*). Furthermore, the computational cost scales up with the spectral resolution for a fixed spectral range, as more variables need to be solved from an increased number of equations.

Spectral response engineering

The second approach to realizing a reconstructive spectrometer is to tailor a distinct spectral response for each of the detectors. This can be achieved either by engineering the detectors themselves or the optical elements integrated on top of the detectors (Fig. 5F). Assuming the spectral response of the ith detector (or the filter-detector pair) to be $D_i(\lambda)$, its measured signal, I_i, can be described as

$$I_i = \int_{\lambda_1}^{\lambda_2} D_i(\lambda) \cdot s(\lambda) d\lambda \qquad (5)$$

The signals of the detector array can then be summarized in a discrete format as

$$\mathbf{I} = \mathbf{D} \cdot \mathbf{S} \qquad (6)$$

where $\mathbf{D}$ is a matrix, the rows of which correspond to the detectors' spectral response functions.

By solving Eq. 6, the unknown target spectrum can be reconstructed. The entire process is illustrated by Fig. 5F. Almost any optical element that can generate diverse spectral response functions can be adopted for spectrometry systems based on this principle, such as quantum dots (*86*, *87*) and photonic crystal slabs (*88*) (Fig. 5, G and H). Other designs including liquid crystals (*89*), thin films (*90*), etalon arrays (*91*), nanostructured photodiodes (*92*, *93*), and metasurfaces (*94*) have also been used as the basis for such strategies. However, all these designs require separate fabrication

of filter and detector arrays. This increases the complexity of manufacturing and limits miniaturization. Recently, spectral responsivity–engineered nanostructure has been demonstrated to integrate both of these functions (*13*, *95*–*99*), as shown in Fig. 5, I and J. For example, a computational spectrometer based on a composition-gradient alloyed semiconductor nanowire was proposed, which can be divided into a number of sections (detectors) along the axial direction (*13*). The response functions of these detectors vary as a result of the gradual and subtle variation in the alloy compositions. Although resolution is still modest (~5 to 10 nm), such a nanowire spectrometer integrates the functions of both wavelength selectivity and photodetection into an individual nanostructure, pushing the footprint toward tens of micrometers, two orders of magnitude below that of any other computational spectrometer system.

However, as the size of the spectrometer decreases, the number of detectors (i.e., the number of equations) that can be accommodated also decreases because of the physical constraints, affecting the ultimate spectral resolution that can be achieved. In addition, the minimized footprint of the spectrometer reduces the light-matter interaction, which compromises sensitivity. In a follow-up work, a nanowire spectrometer was developed that can operate in a waveguide mode, providing an improved signal-to-noise ratio for such an ultracompact device (*96*).

Reconstruction techniques

The inversion problems presented above are typically ill-posed. Different strategies must be adapted to alleviate this, depending on whether the problem is overdetermined or underdetermined—that is, whether the number of detectors (and thus, spectral response functions) is higher or lower than the number of data points in the reconstructed spectrum, respectively. In the overdetermined case, noise in the measurements will be readily amplified into reconstruction errors (*100*). To mitigate this, truncated singular value decomposition can be adopted to remove some part of the measured information that is most easily affected by the noise (*101*). When the problem is underdetermined, additional information such as smoothness should be incorporated to find the most "plausible" solution based on prior knowledge of the type of spectrum being measured (*102*). For example, the original spectrum can be approximated as the combination of a set of smooth basis functions such as Gaussian curves. Compressive sensing has also been adopted to explore the sparseness of the sought spectrum (*103*). According to compressive sensing theory, randomly structured response functions are preferred to improve the spectral resolution as the correlation between the functions is minimized (*88*). Dictionary/machine-learning techniques (*104*) are also promising alternatives to incorporate prior knowledge into the spectral reconstruction process.

Summary and discussion

We have summarized the technological evolution of miniaturized spectrometers, detailing their working principles and merits, under four broad classifications. Despite sharing similar overarching aims, works from these four subfields encompass a hugely diverse range of device designs and operational strategies. Drawing together the field as a whole, Fig. 6A compares the resolution, operational wavelength range, and footprint across the four subcategorizations of device strategies defined above. Clearly, there is a wide variance in performance, footprint, and operational range—even within each subfield—and no platform yet combines high resolution (<1 nm), wide spectral range (>300 nm), and ultracompact physical dimensions (<100 μm). Behind these metrics, it is important to also consider the suitability and ease of integration of each device for different application spaces. For instance, although the MEMS-based system in (*105*) shows competitive resolution performance, wide spectral range, and a small footprint, its complex, 400-μm-tall structure would prove highly challenging for integration into spectrometer arrays such as those required in the snapshot hyperspectral imaging cameras discussed below.

Additionally, the sensitivity of each device design is an increasingly important factor as the detector, and thus the photon collection area, is further reduced in size. This is especially noteworthy given that many portable applications will rely on the collection of ambient light. Here, there are many common factors among the four categories. For instance, the nonintegrated systems discussed above can benefit from the introduction of a lens to focus light onto the detectors, filter array, or dispersive medium (*86*, *106*); enhancing the signal-to-noise ratio of the detectors is also one clear avenue for improvement (*5*). However, there are also a variety of distinct considerations dependent on the device design. In AWG systems, for instance, the overall sensitivity is heavily influenced by the efficiency of coupling light into the waveguide, as well as the dispersion and propagation losses (*15*). As discussed previously, although FT systems benefit from a multiplex advantage in the use of only one detector, transmittance from, for instance, a Fabry-Pérot cavity can be as low as 15% of the incident light (*107*).

Given the need for these devices to function outside controlled laboratory settings, their robustness and stability with respect to their external environment is another operational consideration. In this respect, there are two main impinging factors: changes in temperature and in air composition (for instance, the impact of moisture). Thermal effects are of particular importance where the system is highly sensitive to changes in the refractive index of the active media, for example, in integrated systems such as AWGs, MZIs, and SWIFTSs. Likewise, challenges can arise from the thermal expansion of gratings or MEMS components, as well as through temperature dependencies in the spectral response function of the detectors in computational spectrometers. In many cases, temperature-sensitive calibration can be applied to effectively eliminate (*108*) such effects, and hermetic sealing (*3*) or passivating coatings (*13*) can also be applied to stabilize device performance.

Finally, the relative maturity of these subfields must be taken into account when considering their prospects. To this end, Fig. 6B displays a timeline illustrating the emergence of key design innovations. As may be expected, these milestones have followed wider technological trends; early microspectrometers mainly took advantage of breakthroughs in microfabrication between the 1980s and the early 2000s; advances in lithographic and etch processes, as well as the continued development of MEMS technology and waveguide-based chips, afforded the production of complex miniaturized dispersive, Fourier transform, or filter-based systems.

However, in the past decade, sharp increases in computational power and reductions in processor price and size have seen attention shift toward spectral reconstruction schemes based on relatively simple, and often disordered, device frameworks. We believe these systems represent the most promising paradigm, as their performance can be improved not only by augmenting their hardware but, sometimes more straightforwardly, by optimizing the software that powers them. It seems likely that this trend will continue through further development and optimization of machine learning–based techniques, where the computational power of the accompanying processing systems can shoulder much of the burden for enhancing spectral resolution. As these spectral reconstruction algorithms mature, they will increasingly be able to compensate for the compromises in detector performance necessitated by further miniaturization, allowing for ultracompact yet high-performance systems. Clear hurdles still remain in this respect. For example, deep learning algorithms typically require very large, labeled datasets for proper training of the neural networks used, in order to establish an accurate relationship between the measurements and the spectrum to be reconstructed. In cases where it is challenging to produce sufficient high-quality training data, recent developments in transfer learning

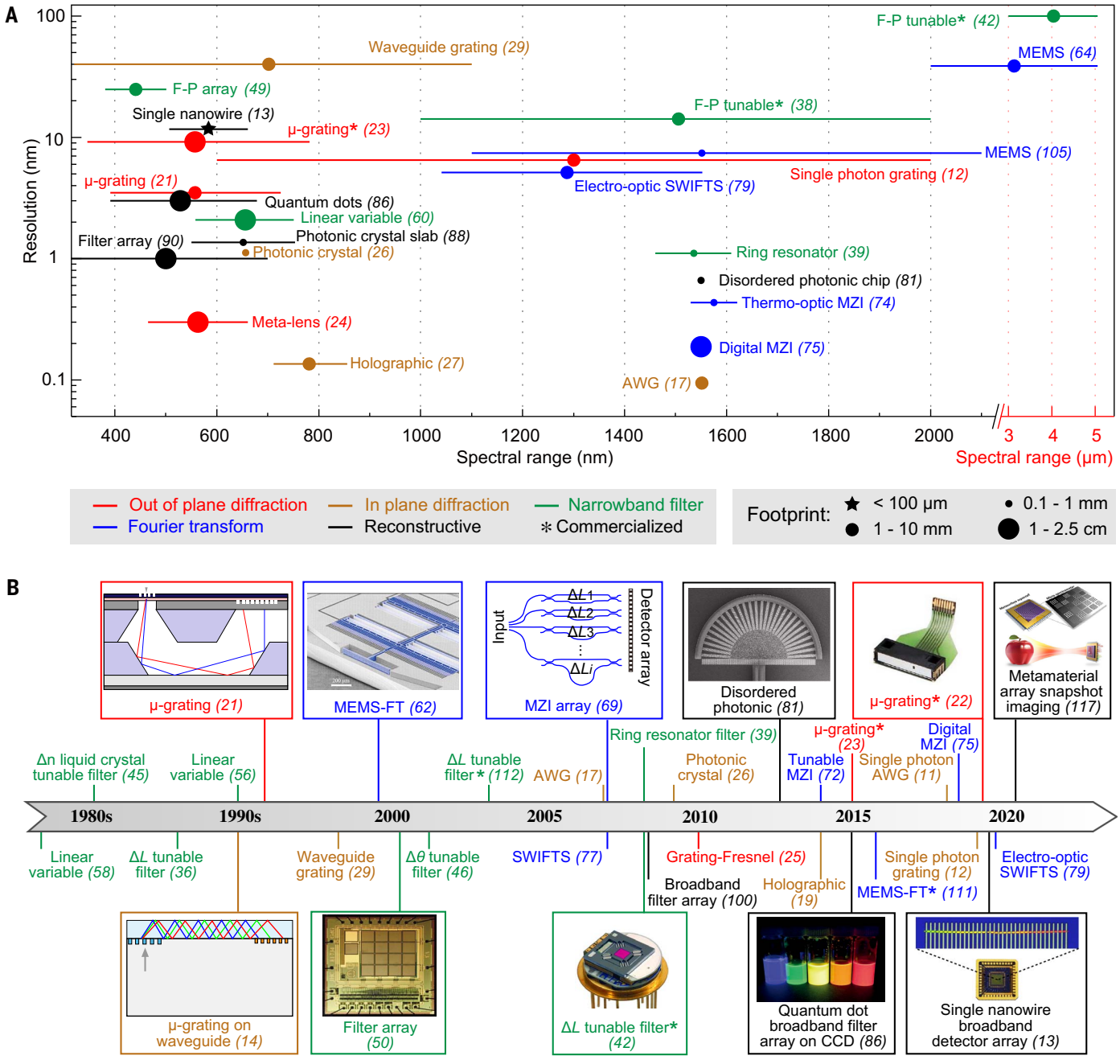

Fig. 6. The field of miniaturized spectroscopic devices. (**A**) Plot comparing the resolution, operational spectral range, and footprint for selected device demonstrations in the literature and those that are commercially available (indicated by asterisks), as categorized into their respective subfields (see color key). Footprint encompasses those elements of the device that are active in resolving and detecting light, and does not include accessory components such as the readout electronics or packaging. Reference numbers are indicated within parentheses. Note that the spectral ranges for (*17*), (*26*), (*75*), and (*81*) (which are obscured by the resolution data points) are 10 nm, 10 nm, 20 nm, and 25 nm, respectively. (**B**) Timeline illustrating the emergence of different technological platforms for microspectrometer systems from the 1980s to the present day, sorted by subfield as displayed in the color key in (A). [Images either redrawn or adapted with permission from the references indicated.]

(*109*, *110*) may provide a solution. Here, knowledge learned from a different but related task is used to improve the performance of the deep learning algorithm for a target task where sufficient training data are not available.

As well as producing more powerful software, further optimization of device hardware must progress in tandem with design of these algorithms, taking into consideration the factors that are most detrimental to their performance. In reconstructive spectrometers, a key issue is noise—that is, inconsistencies between like measurements of the same spectrum. As discussed previously, thermal and environmental sensitivity must be carefully controlled. As made evident by the equations above, more accurate reconstructions should be possible by increasing the number of detectors and the diversity of the spectral response functions, both of which present their own engineering challenges for consideration in the device

architecture. Furthermore, for commercial viability, miniaturization of the charge-coupled device or complementary metal-oxide semiconductor sensors that accompany the filter arrays, as well as associated readout and processing electronics, must also be factored in.

Application outlook

As also seen in Fig. 6, some platforms have already reached full commercial development, showcasing market demand for microspectrometer systems. Over the past two decades, miniaturized, MEMS-based tunable filters and Fourier transform spectrometers as well as centimeter-scale, packaged, grating-based systems have become commercially available (*3*, *22*, *23*, *42*, *111*, *112*). These systems can all be produced with well-established semiconductor device fabrication infrastructure; emerging systems that also fit into these frameworks (such as those based on photonic crystals) have a clear advantage over those where novel manufacturing processes must be developed, such as for nanomaterials-based devices.

More recently, the development of spectral sensing systems embedded within smartphones has been evidenced, at CES (consumer electronics show) 2017 and in patent applications by major smartphone manufacturers, suggesting that an emergence into the public domain may be imminent (*113*, *114*). Indeed, the prospect of a device with a footprint suitable for the smartphone paradigm is arguably the most important factor driving extreme miniaturization of microspectrometer systems; a breakthrough demonstration here could prove pivotal in terms of attracting further attention and investment in this field. Although no reconstructive systems have reached commercial maturity as yet, the readily available processing power, coupled with the need for systems with minimized footprint and weight, make the smartphone platform an obvious area for these microspectrometers to emerge.

Beyond smartphones, we believe that high-performance spectrometry contained within ultraminiaturized packaged systems will find applications in a vast range of fields, industries, and commercial technologies, including satellites and drones, wearables and implantable devices, chemical and food manufacturing, and cellular imaging and lab-on-a-chip systems. The size of ultraminiaturized devices (<100 μm) alone may make them suitable for wearable or flexible technology, given the comparatively large bending radii expected in operation. Array-based devices that already feature flexible, thin-film filters (*86*) could prove promising in this regard if the rigid detectors beneath could be replaced with emerging, flexible counterparts (*115*). Furthermore, bandgap engineering of solution-processable materials (*98*, *99*) could offer a route toward printable, conformable spectrometers.

Perhaps most exciting are the possibilities for hyperspectral imaging applications involving the simultaneous capture of spectral and spatial information in a "data cube" with dimensions (x, y, λ). Here a long-term goal is a miniaturized, portable "snapshot" spectral imager with high spectral and spatial resolution—that is, a camera whereby each pixel holds its own high-performance spectrometer. Such a system would be a marked advance on many current strategies in development, which involve scanning systems with movable parts, or digital mirror device–based spatial light modulators (*116*). Given their simple (and usually planar) device frameworks, as the active sensing area of computational microspectrometers shrinks toward the ~10 μm scale, miniaturized snapshot imagers based on such concepts become increasingly feasible. Indeed, successful prototypes based on arrays of "superpixels," each containing their own filter array, have very recently been reported (*117*, *118*). The addition of a diffuser here can convey a multiplexing advantage whereby each point in the object plane is mapped to many different points (rather than one point, as with a lens) at the superpixel array (*118*). Besides consumer technology, such devices could potentially revolutionize existing hyperspectral imaging applications in agriculture and mineralogy.

REFERENCES AND NOTES

1. C. P. Bacon, Y. Mattley, R. DeFrece, Miniature spectroscopic instrumentation: Applications to biology and chemistry. *Rev. Sci. Instrum.* **75**, 1–16 (2004). doi: 10.1063/1.1633025
2. L. P. Schuler, J. S. Milne, J. M. Dell, L. Faraone, MEMS-based microspectrometer technologies for NIR and MIR wavelengths. *J. Phys. D* **42**, 133001 (2009). doi: 10.1088/0022-3727/42/13/133001
3. J. Malinen *et al*., Advances in miniature spectrometer and sensor development. *Proc. SPIE* **9101**, 91010C (2014). doi: 10.1117/12.2053567
4. M. Ebermann *et al*., Tunable MEMS Fabry-Pérot filters for infrared microspectrometers: A review. *Proc. SPIE* **9760**, 97600H (2016). doi: 10.1117/12.2209288
5. R. A. Crocombe, Portable Spectroscopy. *Appl. Spectrosc.* **72**, 1701–1751 (2018). doi: 10.1177/0003702818809719; pmid: 30335465
6. R. F. Wolffenbuttel, MEMS-based optical mini- and microspectrometers for the visible and infrared spectral range. *J. Micromech. Microeng.* **15**, S145–S152 (2005). doi: 10.1088/0960-1317/15/7/021
7. M. Manley, Near-infrared spectroscopy and hyperspectral imaging: Non-destructive analysis of biological materials. *Chem. Soc. Rev.* **43**, 8200–8214 (2014). doi: 10.1039/C4CS00062E; pmid: 25156745
8. A. J. S. McGonigle *et al*., Smartphone Spectrometers. *Sensors* **18**, 223 (2018). doi: 10.3390/s18010223; pmid: 29342899
9. P. Edwards *et al*., Smartphone based optical spectrometer for diffusive reflectance spectroscopic measurement of hemoglobin. *Sci. Rep.* **7**, 12224 (2017). doi: 10.1038/s41598-017-12482-5; pmid: 28939898
10. E. Ryckeboer, R. Bockstaele, M. Vanslembrouck, R. Baets, Glucose sensing by waveguide-based absorption spectroscopy on a silicon chip. *Biomed. Opt. Express* **5**, 1636–1648 (2014). doi: 10.1364/BOE.5.001636; pmid: 24877021
11. V. Kovalyuk *et al*., On-chip single-photon spectrometer for visible and infrared wavelength range. *J. Phys. Conf. Ser.* **1124**, 051045 (2018). doi: 10.1088/1742-6596/1124/5/051045
12. R. Cheng *et al*., Broadband on-chip single-photon spectrometer. *Nat. Commun.* **10**, 4104 (2019). doi: 10.1038/s41467-019-12149-x; pmid: 31506440
13. Z. Yang *et al*., Single-nanowire spectrometers. *Science* **365**, 1017–1020 (2019). doi: 10.1126/science.aax8814; pmid: 31488686
14. D. S. Goldman, P. L. White, N. C. Anheier, Miniaturized spectrometer employing planar waveguides and grating couplers for chemical analysis. *Appl. Opt.* **29**, 4583–4589 (1990). doi: 10.1364/AO.29.004583; pmid: 20577437
15. A. Z. Subramanian *et al*., Silicon and silicon nitride photonic circuits for spectroscopic sensing on-a-chip. *Photon. Res.* **3**, B47 (2015). doi: 10.1364/PRJ.3.000B47
16. D. Sander, J. Muller, Selffocussing phase transmission grating for an integrated optical microspectrometer. *Sens. Actuators A* **88**, 1–9 (2001). doi: 10.1016/S0924-4247(00)00499-4
17. P. Cheben *et al*., A high-resolution silicon-on-insulator arrayed waveguide grating microspectrometer with sub-micrometer aperture waveguides. *Opt. Express* **15**, 2299–2306 (2007). doi: 10.1364/OE.15.002299; pmid: 19532464
18. B. Gao, Z. Shi, R. W. Boyd, Design of flat-band superprism structures for on-chip spectroscopy. *Opt. Express* **23**, 6491–6496 (2015). doi: 10.1364/OE.23.006491; pmid: 25836867
19. G. Calafiore *et al*., Holographic planar lightwave circuit for on-chip spectroscopy. *Light Sci. Appl.* **3**, e203 (2014). doi: 10.1038/lsa.2014.84
20. R. F. Wolffenbuttel, State-of-the-art in integrated optical microspectrometers. *IEEE Trans. Instrum. Meas.* **53**, 197–202 (2004). doi: 10.1109/TIM.2003.821490
21. T. A. Kwa, R. F. Wolffenbuttel, Integrated grating/detector array fabricated in silicon using micromachining techniques. *Sens. Actuators A* **31**, 259–266 (1992). doi: 10.1016/0924-4247(92)80114-I
22. T. Yokino *et al*., Grating-based ultra-compact SWNIR spectral sensor head developed through MOEMS technology. *Proc. SPIE* **10931**, 8 (2019). doi: 10.1117/12.2510472
23. Hamamatsu mini-spectrometer micro series C12666MA (2015); www.hamamatsu.com/jp/en/product/type/C12666MA/index.html.
24. A. Y. Zhu *et al*., Ultra-compact visible chiral spectrometer with meta-lenses. *APL Photon.* **2**, 036103 (2017). doi: 10.1063/1.4974259
25. C. Yang, K. Shi, P. Edwards, Z. Liu, Demonstration of a PDMS based hybrid grating and Fresnel lens (G-Fresnel) device. *Opt. Express* **18**, 23529–23534 (2010). doi: 10.1364/OE.18.023529; pmid: 21164696
26. B. Momeni, E. S. Hosseini, A. Adibi, Planar photonic crystal microspectrometers in silicon-nitride for the visible range. *Opt. Express* **17**, 17060–17069 (2009). doi: 10.1364/OE.17.017060; pmid: 19770924
27. A. Koshelev *et al*., Combination of a spectrometer-on-chip and an array of Young's interferometers for laser spectrum monitoring. *Opt. Lett.* **39**, 5645–5648 (2014). doi: 10.1364/OL.39.005645; pmid: 25360949
28. J.-J. He *et al*., Monolithic integrated wavelength demultiplexer based on a waveguide Rowland circle grating in InGaAsP/InP. *J. Lightwave Technol.* **16**, 631–638 (1998). doi: 10.1109/50.664075
29. D. Sander, M.-O. Duecker, O. Blume, J. Mueller, An optical microspectrometer in SiON-slab-waveguides. *Proc. SPIE* **2686**, 100–107 (1996). doi: 10.1117/12.236128
30. S. Nezhadbadeh, A. Neumann, P. Zarkesh-Ha, S. R. J. Brueck, Chirped-grating spectrometer-on-a-chip. *Opt. Express* **28**, 24501–24510 (2020). doi: 10.1364/OE.398072; pmid: 32906990
31. M. Faraji-Dana *et al*., Compact folded metasurface spectrometer. *Nat. Commun.* **9**, 4196 (2018). doi: 10.1038/s41467-018-06495-5; pmid: 30305616
32. S. Janz *et al*., Planar waveguide echelle gratings in silica-on-silicon. *IEEE Photonics Technol. Lett.* **16**, 503–505 (2004). doi: 10.1109/LPT.2003.823139
33. J. Zou, T. Lang, Z. Le, J. J. He, Ultracompact silicon-on-insulator-based reflective arrayed waveguide gratings for spectroscopic applications. *Appl. Opt.* **55**, 3531–3536 (2016). doi: 10.1364/AO.55.003531; pmid: 27140366
34. H. Y. Zhang, X. L. Wang, J. Soos, J. Crisp, Design of a miniature solid-state NIR spectrometer. *Proc. SPIE* **2475**, 376–383 (1995). doi: 10.1117/12.211276
35. N. Gat, Imaging spectroscopy using tunable filters: A review. *Proc. SPIE* **4056**, 50–64 (2000). doi: 10.1117/12.381686
36. S. R. Mallinson, J. H. Jerman, Miniature micromachined Fabry-Perot interferometers in silicon. *Electron. Lett.* **23**, 1041 (1987). doi: 10.1049/el:19870728
37. J. P. Carmo *et al*., A review of visible-range Fabry-Perot microspectrometers in silicon for the industry. *Opt. Laser*

Technol. **44**, 2312–2320 (2012). doi: 10.1016/j.optlastec.2012.03.036

38. J. Antila *et al*., MEMS and piezo actuator-based Fabry-Perot interferometer technologies and applications at VTT. *Proc. SPIE* **7680**, 76800U (2010). doi: 10.1117/12.850164
39. A. Nitkowski, L. Chen, M. Lipson, Cavity-enhanced on-chip absorption spectroscopy using microring resonators. *Opt. Express* **16**, 11930–11936 (2008). doi: 10.1364/OE.16.011930; pmid: 18679466
40. P. M. Zavracky, E. Hennenberg, Miniature Fabry Perot spectrometers using micromachining technology. *Proc. WESCON* **95**, 325–332 (1995). doi: 10.1109/WESCON.1995.485299
41. J. H. Jerman, D. J. Clift, S. R. Mallinson, A miniature Fabry-Perot-interferometer with a corrugated silicon diaphragm support. *Sens. Actuators A* **29**, 151–158 (1991). doi: 10.1016/0924-4247(91)87117-L
42. N. Neumann, M. Ebermann, S. Kurth, K. Hiller, Tunable infrared detector with integrated micromachined Fabry-Perot filter. *J. Micro-Nanolith. MEM* **7**, 021004 (2008).
43. W. J. Gunning, P. Yeh, Multiple-cavity infrared electro-optic tunable filter. *Proc. SPIE* **0202**, 21–25 (1980). doi: 10.1117/12.958092
44. Y. Yao *et al*., Design of programmable multi-wavelength tunable filter on lithium niobate. *Results Phys.* **15**, 102741 (2019). doi: 10.1016/j.rinp.2019.102741
45. W. Gunning, J. Pasko, J. Tracy, A liquid crystal tunable spectral filter: Visible and infrared operation. *Proc. SPIE* **0268**, 190–194 (1981). doi: 10.1117/12.959943
46. G. Lammel, S. Schweizer, P. Renaud, Microspectrometer based on a tunable optical filter of porous silicon. *Sens. Actuators A* **92**, 52–59 (2001). doi: 10.1016/S0924-4247(01)00539-8
47. J.-H. Liao, W. Wang, C.-J. Chen, C.-J. Yu, M.-C. Wu, Design and fabrication of large-area tunable MOEMS-based shortwave infrared Fabry-Pérot filters. *J. Vac. Sci. Technol. B* **37**, 032002 (2019). doi: 10.1116/1.5085259
48. P. J. Lapray, X. Wang, J. B. Thomas, P. Gouton, Multispectral filter arrays: Recent advances and practical implementation. *Sensors* **14**, 21626–21659 (2014). doi: 10.3390/s141121626; pmid: 25407904
49. J. H. Correia, G. de Graaf, S. H. Kong, M. Bartek, R. F. Wolffenbuttel, Single-chip CMOS optical microspectrometer. *Sens. Actuators A* **82**, 191–197 (2000). doi: 10.1016/S0924-4247(99)00369-6
50. S.-H. Kong, J. H. Correia, G. de Graaf, M. Bartek, R. F. Wolffenbuttel, Integrated silicon microspectrometers. *IEEE Instrum. Meas. Mag.* **4**, 34–38 (2001). doi: 10.1109/5289.953457
51. S. W. Wang *et al*., Concept of a high-resolution miniature spectrometer using an integrated filter array. *Opt. Lett.* **32**, 632–634 (2007). doi: 10.1364/OL.32.000632; pmid: 17308584
52. N. K. Pervez *et al*., Photonic crystal spectrometer. *Opt. Express* **18**, 8277–8285 (2010). doi: 10.1364/OE.18.008277; pmid: 20588673
53. Q. Hang, B. Ung, I. Syed, N. Guo, M. Skorobogatiy, Photonic bandgap fiber bundle spectrometer. *Appl. Opt.* **49**, 4791–4800 (2010). doi: 10.1364/AO.49.004791; pmid: 20820222
54. A. Tittl *et al*., Imaging-based molecular barcoding with pixelated dielectric metasurfaces. *Science* **360**, 1105–1109 (2018). doi: 10.1126/science.aas9768; pmid: 29880685
55. A. Thelen, Circularly wedged optical coatings I: Theory. *Appl. Opt.* **4**, 977 (1965). doi: 10.1364/AO.4.000977
56. A. M. Mika, Linear-wedge spectrometer. *Proc. SPIE* **1298**, 127–131 (1990). doi: 10.1117/12.21343
57. M. Grundmann, Modeling of a waveguide-based UV-VIS-IR spectrometer based on a lateral (In,Ga)N alloy gradient. *Phys. Status Solidi A* **216**, 1900170 (2019). doi: 10.1002/pssa.201900170
58. W. A. Hovis Jr.., W. A. Kley, M. G. Strange, Filter wedge spectrometer for field use. *Appl. Opt.* **6**, 1057–1058 (1967). doi: 10.1364/AO.6.001057; pmid: 20062123
59. O. Pust, Innovative filter solutions for hyperspectral imaging. *Optik Photon.* **11**, 24–27 (2016). doi: 10.1002/opph.201600012
60. A. Emadi, H. Wu, G. de Graaf, R. Wolffenbuttel, Design and implementation of a sub-nm resolution microspectrometer based on a Linear-Variable Optical Filter. *Opt. Express* **20**, 489–507 (2012). doi: 10.1364/OE.20.000489; pmid: 22274371
61. R. G. DeCorby, N. Ponnampalam, E. Epp, T. Allen, J. N. McMullin, Chip-scale spectrometry based on tapered hollow Bragg waveguides. *Opt. Express* **17**, 16632–16645 (2009). doi: 10.1364/OE.17.016632; pmid: 19770879
62. O. Manzardo, H. P. Herzig, C. R. Marxer, N. F. de Rooij, Miniaturized time-scanning Fourier transform spectrometer based on silicon technology. *Opt. Lett.* **24**, 1705–1707 (1999). doi: 10.1364/OL.24.001705; pmid: 18079909
63. M. Erfan *et al*., On-chip micro-electro-mechanical system Fourier transform infrared (MEMS FT-IR) spectrometer-based gas sensing. *Appl. Spectrosc.* **70**, 897–904 (2016). doi: 10.1177/0003702816638295; pmid: 27044847
64. T. Sandner, A. Kenda, C. Drabe, H. Schenk, W. Scherf, Miniaturized FTIR-spectrometer based on optical MEMS translatory actuator. *Proc. SPIE* **6466**, 646602 (2007). doi: 10.1117/12.697898
65. U. Wallrabe, C. Solf, J. Mohr, J. G. Korvink, Miniaturized Fourier Transform spectrometer for the near infrared wavelength regime incorporating an electromagnetic linear actuator. *Sens. Actuators A* **123–124**, 459–467 (2005). doi: 10.1016/j.sna.2005.05.014
66. W. Wang, S. R. Samuelson, J. Chen, H. Xie, Miniaturizing Fourier transform spectrometer with an electrothermal micromirror. *IEEE Photonics Technol. Lett.* **27**, 1418–1421 (2015). doi: 10.1109/LPT.2015.2423637
67. K. Wang, J. Li, D. F. Lu, Z. M. Qi, Algorithmic enhancement of spectral resolution of a $LiNbO_3$ waveguide-based miniature Fourier transform spectrometer. *Appl. Spectrosc.* **70**, 1685–1691 (2016). doi: 10.1177/0003702816644454; pmid: 27402687
68. P. Malara *et al*., A self-operating broadband spectrometer on a droplet. *Nat. Commun.* **11**, 2263 (2020). doi: 10.1038/s41467-020-16206-8; pmid: 32385273
69. M. Florjańczyk *et al*., Multiaperture planar waveguide spectrometer formed by arrayed Mach-Zehnder interferometers. *Opt. Express* **15**, 18176–18189 (2007). doi: 10.1364/OE.15.018176; pmid: 19551116
70. A. V. Velasco *et al*., High-resolution Fourier-transform spectrometer chip with microphotonic silicon spiral waveguides. *Opt. Lett.* **38**, 706–708 (2013). doi: 10.1364/OL.38.000706; pmid: 23455272
71. H. Podmore *et al*., Demonstration of a compressive-sensing Fourier-transform on-chip spectrometer. *Opt. Lett.* **42**, 1440–1443 (2017). doi: 10.1364/OL.42.001440; pmid: 28362792
72. J. Li, D. F. Lu, Z. M. Qi, Miniature Fourier transform spectrometer based on wavelength dependence of half-wave voltage of a $LiNbO_3$ waveguide interferometer. *Opt. Lett.* **39**, 3923–3926 (2014). doi: 10.1364/OL.39.003923; pmid: 24978772
73. M. C. M. M. Souza, A. Grieco, N. C. Frateschi, Y. Fainman, Fourier transform spectrometer on silicon with thermo-optic non-linearity and dispersion correction. *Nat. Commun.* **9**, 665 (2018). doi: 10.1038/s41467-018-03004-6; pmid: 29445152
74. S. N. Zheng *et al*., Microring resonator-assisted Fourier transform spectrometer with enhanced resolution and large bandwidth in single chip solution. *Nat. Commun.* **10**, 2349 (2019). doi: 10.1038/s41467-019-10282-1; pmid: 31138800
75. D. M. Kita *et al*., High-performance and scalable on-chip digital Fourier transform spectroscopy. *Nat. Commun.* **9**, 4405 (2018). doi: 10.1038/s41467-018-06773-2; pmid: 30353014
76. A. Herrero-Bermello *et al*., On-chip Fourier-transform spectrometers and machine learning: A new route to smart photonic sensors. *Opt. Lett.* **44**, 5840–5843 (2019). doi: 10.1364/OL.44.005840; pmid: 31774793
77. E. le Coarer *et al*., Wavelength-scale stationary-wave integrated Fourier-transform spectrometry. *Nat. Photonics* **1**, 473–478 (2007). doi: 10.1038/nphoton.2007.138
78. X. Nie, E. Ryckeboer, G. Roelkens, R. Baets, CMOS-compatible broadband co-propagative stationary Fourier transform spectrometer integrated on a silicon nitride photonics platform. *Opt. Express* **25**, A409–A418 (2017). doi: 10.1364/OE.25.00A409; pmid: 28437970
79. D. Pohl *et al*., An integrated broadband spectrometer on thin-film lithium niobate. *Nat. Photonics* **14**, 24–29 (2020). doi: 10.1038/s41566-019-0529-9
80. B. Redding, S. M. Popoff, H. Cao, All-fiber spectrometer based on speckle pattern reconstruction. *Opt. Express* **21**, 6584–6600 (2013). doi: 10.1364/OE.21.006584; pmid: 23482230
81. B. Redding, S. F. Liew, R. Sarma, H. Cao, Compact spectrometer based on a disordered photonic chip. *Nat. Photonics* **7**, 746–751 (2013). doi: 10.1038/nphoton.2013.190
82. W. Hartmann *et al*., Waveguide-Integrated Broadband Spectrometer Based on Tailored Disorder. *Adv. Opt. Mater.* **8**, 1901602 (2020). doi: 10.1002/adom.201901602
83. B. Redding, S. Fatt Liew, Y. Bromberg, R. Sarma, H. Cao, Evanescently coupled multimode spiral spectrometer. *Optica* **3**, 956 (2016). doi: 10.1364/OPTICA.3.000956
84. T. Yang *et al*., Miniature spectrometer based on diffraction in a dispersive hole array. *Opt. Lett.* **40**, 3217–3220 (2015). doi: 10.1364/OL.40.003217; pmid: 26125406
85. P. Wang, R. Menon, Computational spectrometer based on a broadband diffractive optic. *Opt. Express* **22**, 14575–14587 (2014). doi: 10.1364/OE.22.014575; pmid: 24977553
86. J. Bao, M. G. Bawendi, A colloidal quantum dot spectrometer. *Nature* **523**, 67–70 (2015). doi: 10.1038/nature14576; pmid: 26135449
87. X. Zhu *et al*., Broadband perovskite quantum dot spectrometer beyond human visual resolution. *Light Sci. Appl.* **9**, 73 (2020). doi: 10.1038/s41377-020-0301-4; pmid: 32377335
88. Z. Wang *et al*., Single-shot on-chip spectral sensors based on photonic crystal slabs. *Nat. Commun.* **10**, 1020 (2019). doi: 10.1038/s41467-019-08994-5; pmid: 30833569
89. Y. August, A. Stern, Compressive sensing spectrometry based on liquid crystal devices. *Opt. Lett.* **38**, 4996–4999 (2013). doi: 10.1364/OL.38.004996; pmid: 24281493
90. J. Oliver, W. B. Lee, H. N. Lee, Filters with random transmittance for improving resolution in filter-array-based spectrometers. *Opt. Express* **21**, 3969–3989 (2013). doi: 10.1364/OE.21.003969; pmid: 23481932
91. E. Huang, Q. Ma, Z. Liu, Etalon array reconstructive spectrometry. *Sci. Rep.* **7**, 40693 (2017). doi: 10.1038/srep40693; pmid: 28074883
92. A. Ahamad *et al*., Smart nanophotonics silicon spectrometer array for hyperspectral imaging. *CLEO*, STh3M.2 (2020). doi: 10.1364/CLEO_SI.2020.STh3M.2
93. Y. Gao *et al*., Photon-trapping microstructures enable high-speed high-efficiency silicon photodiodes. *Nat. Photonics* **11**, 301–308 (2017). doi: 10.1038/nphoton.2017.37
94. B. Craig, V. R. Shrestha, J. Meng, J. J. Cadusch, K. B. Crozier, Experimental demonstration of infrared spectral reconstruction using plasmonic metasurfaces. *Opt. Lett.* **43**, 4481–4484 (2018). doi: 10.1364/OL.43.004481; pmid: 30211895
95. J. Meng, J. J. Cadusch, K. B. Crozier, Detector-only spectrometer based on structurally colored silicon nanowires and a reconstruction algorithm. *Nano Lett.* **20**, 320–328 (2020). doi: 10.1021/acs.nanolett.9b03862; pmid: 31829611
96. B. Zheng *et al*., On-chip measurement of photoluminescence with high sensitivity monolithic spectrometer. *Adv. Opt. Mater.* **8**, 2000191 (2020). doi: 10.1002/adom.202000191
97. J. Dong, The smallest nanowire spectrometers. *Front Optoelectron.* **12**, 341 (2020). doi: 10.1007/s12200-019-0983-5
98. M.-N. Zhang *et al*., Spectrum projection with a bandgap-gradient perovskite cell for colour perception. *Light Sci. Appl.* **9**, 162 (2020). doi: 10.1038/s41377-020-00400-w; pmid: 33014357
99. H. Sun *et al*., In Situ Formed Gradient Bandgap-Tunable Perovskite for Ultrahigh-Speed Color/Spectrum-Sensitive Photodetectors via Electron-Donor Control. *Adv. Mater.* **32**, e1908108 (2020). doi: 10.1002/adma.201908108; pmid: 32080927
100. C. C. Chang, H. N. Lee, On the estimation of target spectrum for filter-array based spectrometers. *Opt. Express* **16**, 1056–1061 (2008). doi: 10.1364/OE.16.001056; pmid: 18542178
101. P. C. Hansen, *Rank-Deficient and Discrete Ill-Posed Problems* (SIAM, 2005), vol. 4.
102. C.-C. Chang, H.-Y. Lin, Spectrum reconstruction for on-chip spectrum sensor array using a novel blind nonuniformity correction method. *IEEE Sens. J.* **12**, 2586–2592 (2012). doi: 10.1109/JSEN.2012.2197609
103. Z. Wang, Z. Yu, Spectral analysis based on compressive sensing in nanophotonic structures. *Opt. Express* **22**, 25608–25614 (2014). doi: 10.1364/OE.22.025608; pmid: 25401594
104. S. Zhang, Y. Dong, H. Fu, S. L. Huang, L. Zhang, A spectral reconstruction algorithm of miniature spectrometer based on sparse optimization and dictionary learning. *Sensors* **18**, 644 (2018). doi: 10.3390/s18020644; pmid: 29470406
105. Y. M. Eltagoury, Y. M. Sabry, D. A. Khalil, All-silicon double-cavity Fourier-transform infrared spectrometer on-chip. *Adv. Mater. Technol.* **4**, 1900441 (2019). doi: 10.1002/admt.201900441

106. R. Mannila *et al*., Gas detection with microelectromechanical Fabry-Perot interferometer technology in cell phone. *Proc. SPIE* **9482**, 94820P (2015). doi: 10.1117/12.2176923
107. J. H. Correia, M. Bartek, R. F. Wolffenbuttel, High-selectivity single-chip spectrometer in silicon for operation at visible part of the spectrum. *IEEE Trans. Electron Dev.* **47**, 553–559 (2000). doi: 10.1109/16.824727
108. A. Herrero-Bermello *et al*., Temperature dependence mitigation in stationary Fourier-transform on-chip spectrometers. *Opt. Lett.* **42**, 2239–2242 (2017). doi: 10.1364/OL.42.002239; pmid: 28569891
109. D. Jha *et al*., Enhancing materials property prediction by leveraging computational and experimental data using deep transfer learning. *Nat. Commun.* **10**, 5316 (2019). doi: 10.1038/s41467-019-13297-w; pmid: 31757948
110. J. S. Smith *et al*., Approaching coupled cluster accuracy with a general-purpose neural network potential through transfer learning. *Nat. Commun.* **10**, 2903 (2019). doi: 10.1038/s41467-019-10827-4; pmid: 31263102
111. NeoSpectra-micro FTIR (2016); www.neospectra.com/our-offerings/neospectra-micro/.
112. P. Kotidis *et al*., Optical, tunable filter-based micro-instrumentation for industrial applications. *Proc. Instr. Syst. and Autom. Soc. (ISA)*, (2003). www.thevespiary.org/library/Files_Uploaded_by_Users/no1uno/pdf/Instrumentation/IR/Kotidis.etal.Optical.Tunable.Filter.Based.Micro.Instrumentation.for.Industrial.Applications.pdf.
113. Changhong H2 spectrometer phone (2017); www.cnet.com/pictures/changhong-h2-ces-2017/3/.
114. Electronic device comprising plurality of light sources. U.S. Patent 20190290148A1 (2018).
115. A. Koppelhuber, O. Bimber, Towards a transparent, flexible, scalable and disposable image sensor using thin-film luminescent concentrators. *Opt. Express* **21**, 4796–4810 (2013). doi: 10.1364/OE.21.004796; pmid: 23482014
116. N. Hagen, M. W. Kudenov, Review of snapshot spectral imaging technologies. *Opt. Eng.* **52**, 090901 (2013). doi: 10.1117/1.OE.52.9.090901
117. X. Cai *et al*., One-shot ultraspectral imaging with reconfigurable metasurfaces. arXiv 2005.02689 [physics.optics] (7 May 2020).
118. K. Monakhova, K. Yanny, N. Aggarwal, L. Waller, Spectral DiffuserCam: Lensless snapshot hyperspectral imaging with a spectral filter array. *Optica* **7**, 1298 (2020). doi: 10.1364/OPTICA.397214

ACKNOWLEDGMENTS

We thank W. Han for valuable discussions. **Funding:** Supported by the National Natural Science Foundation of China (51706141, 51976122) and EPSRC (EP/L016087/1, EP/T014601/1). **Competing interests:** The authors declare no competing interests.

10.1126/science.abe0722

Science

Miniaturization of optical spectrometers

Zongyin Yang, Tom Albrow-Owen, Weiwei Cai and Tawfique Hasan

Science **371** (6528), eabe0722.
DOI: 10.1126/science.abe0722

Miniaturizing spectrometers

Optical spectroscopy is a widely used characterization tool in industrial and research laboratory settings for chemical fingerprinting and analysis. High-end spectrometers are typically benchtop based with bulky optical components, moving parts, and long path lengths, and they can deliver a wealth of information with ultrahigh precision and bandwidth. There is, however, a drive toward miniaturization of spectrometers, in which concepts in nanophotonics are used to control light on much smaller scales. Yang *et al.* reviewed recent developments in spectrometry systems, including various fabrication approaches of nanophotonics systems and the software that computationally determines the spectra, that strive to shrink their footprint and open up applications in portable spectroscopy.

Science, this issue p. eabe0722